Molecular dynamics simulations of hydrogen bonding in clathrate hydrates with ammonia and methanol guest molecules

Alavi, Saman; Shin, Kyuchul; Ripmeester, John A.

Publisher's version / Version de l'éditeur:
https://doi.org/10.1021/je5006517
Journal of Chemical and Engineering Data, 60, 2, pp. 389-397, 2014-09-18

Journal of chemical & engineering data

Article

pubs.acs.org/jced

Molecular Dynamics Simulations of Hydrogen Bonding in Clathrate Hydrates with Ammonia and Methanol Guest Molecules

Saman Alavi,*[,†,‡] Kyuchul Shin,[§] and John A. Ripmeester*[,†,‡]

[†]National Research Council of Canada, 100 Sussex Dr., Ottawa, Ontario K1N 0R6, Canada

[‡]Department of Chemical and Biological Engineering, University of British Columbia, Vancouver, British Columbia V6T 1Z3, Canada

[§]Department of Applied Chemistry, Kyungpook National University, Daegu, 702-701, Republic of Korea

Supporting Information

ABSTRACT: We performed molecular dynamics simulations of the ammonia and methanol-based clathrate hydrates with the emphasis on characterizing hydrogen-bonding interactions of these guest molecules with the water lattice. Systems studied include structure II (sII) binary clathrate hydrates of tetrahydrofuran (THF) (large cage, L) + NH_3 (small cage, S) and THF (L) + CH_3OH (S), the structure I (sI) pure NH_3 (L), pure CH_3OH (L), the binary NH_3 (L) + CH_4 (S), and binary CH_3OH (L) + CH_4 (S) clathrate hydrates. We simulated these clathrate hydrates with the transferable intermolecular potential with four point changes (TIP4P) water potential and the TIP4P/ice water potential to determine the effect of the water potential on the predicted hydrogen bonding of the guest molecules. Simulations show that, despite strongly hydrogen bonding with the framework water molecules, clathrate hydrate phases with NH_3 and CH_3OH can be stable within temperatures ranges up to 240 K. Indeed, a limited number of thermodynamic integration free energy calculations show that both NH_3 and CH_3OH molecules give more stable guest−host configurations in the large sI clathrate hydrate cages than methane guests. Predictions of hydrogen bonding from simulations with the two different water potentials used can differ substantially. To study the effect of proton transfer from water to the basic NH_3 guests, simulations were performed on a binary NH_3 + CH_4 sI clathrate hydrate where less than 10 % of the ammonia guests in the large cages were converted to NH_4^+ and a water molecule of the hydrate lattice in the same large cage was converted to OH^-. The small percentage of proton transfer to ammonia guests in the large cages did not affect the stability of the resultant hydrate. The structural perturbations in the lattice that result from this proton transfer are characterized.

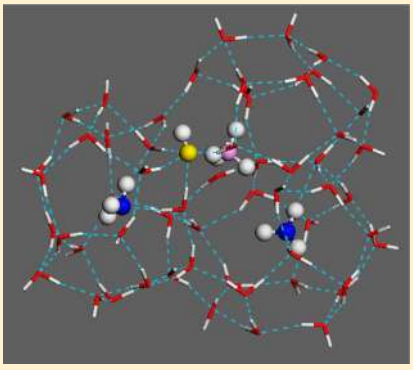

INTRODUCTION

While many clathrate hydrates of water-miscible[1−3] hydrogen-bonding guests[4−7] such as tetrahydrofuran (THF) are known, small polar molecules such as methanol (and other lower alcohols) and ammonia are traditionally considered to be inhibitors of clathrate hydrate formation. Indeed methanol is used in large quantities in oil and natural gas pipelines as a thermodynamic hydrate inhibitor, and its use underlies the engineering field of pipeline flow assurance.[8] The fact that clathrate hydrate formation is not observed for aqueous solutions of these solute molecules is interpreted in terms of the instability of the clathrate hydrate phases of these guests and the inherent stability of the aqueous solutions of the water-miscible substances. However, the small polar NH_3 and CH_3OH molecules can form nonstoichiometric hydrate phases from ice in the presence of methane or from aqueous solutions of THF.[9,10] The synthetic routes include clathrate hydrate synthesis via vapor deposition of water and gaseous guests, direct synthesis of binary hydrates from aqueous THF solutions with either ammonia or methanol, and synthesis of hydrates from frozen aqueous methanol or ammonia solutions and gaseous guests in the presence of methane or propane.

The binary structure II (sII) clathrate hydrates with THF as the large cage guest and ammonia or methanol as the small cage guests have been synthesized directly from cold aqueous THF solutions and single crystal X-ray structures of these phases have verified the presence of ammonia or methanol in the small cages of the sII phases. Pure structure I (sI) clathrate hydrates of NH_3 and a mixture of sI and sII binary NH_3 + CH_4 hydrates have been synthesized by vapor codeposition of the gases and water vapor at ∼20 K and annealing between ∼125 and 150 K (under vacuum, or under CH_4 pressure in the case of binary hydrates).[9] Under similar conditions, pure methanol hydrate did not form, but a complex mixture of sI and a mixed layer form of sII and structure H (sH) binary clathrate hydrates of methanol and methane are formed when vapor codeposited methanol and water are exposed to pressures of methane gas.[10] The presence of ammonia and methanol in clathrate hydrate

Special Issue: In Honor of E. Dendy Sloan on the Occasion of His 70th Birthday

Received: July 11, 2014
Accepted: September 8, 2014
Published: September 18, 2014

cages has been demonstrated by single-crystal X-ray diffraction studies, powder X-ray diffraction (PXRD), NMR studies, and molecular dynamics simulations. As well, complex ternary sI clathrate hydrate phases have been synthesized from water/NH_4F/methanol system.[11] Diffraction analysis for structural determination and ^2H NMR spectroscopy showed that methanol can be a guest in the cages of this clathrate hydrate phase.

In this work we perform detailed molecular dynamics simulations of ammonia- and methanol-containing clathrate hydrates with the emphasis on characterizing ammonia and methanol hydrogen-bonding interactions with clathrate hydrate water phase. Simulations show that clathrate hydrates of NH_3 and CH_3OH, while showing extensive hydrogen bonding between the guests and water from the hydrate framework, can be stable. This work strengthens the assumption that the clathrate hydrate inhibition effect of ammonia and methanol in aqueous solution, under a sufficient pressure of hydrocarbon gases, is related to the thermodynamic stability of the aqueous solutions and not the inherent instability of the solid-phase clathrate hydrate of NH_3 and CH_3OH.

Clathrate hydrates studied in this work include the sII THF + NH_3 and THF + CH_3OH clathrate hydrates, the sI pure NH_3, pure sI CH_3OH, binary sI NH_3 + CH_4, and binary sI CH_3OH + CH_4 clathrate hydrates. We also study the stability of the sI NH_3 + NH_4OH clathrate hydrate, where less than 10 % of the NH_3 in the large sI cages have been replaced by NH_4^+ cations and one of the water molecules of the corresponding large cage is converted to OH^-. This latter simulation mimics the effect of proton transfer from water to NH_3 as temperatures of the clathrate hydrate are raised.

We study the effect of the water force field on the predicted amount of hydrogen bonding of these two guests by performing two sets of simulations with the widely used TIP4P potential[12] and the TIP4P/ice potential.[13] The TIP4P/ice potential predicts a more accurate melting point for ice and decomposition temperatures for methane hydrate. Wide differences in the observed hydrogen bonding between these two water potentials could lead to methodological preference of the use of one over the other.

COMPUTATIONAL METHODS

Molecular dynamics simulations are performed with DL_POLY version 2.20[14] using the leapfrog algorithm with a time step of 1 fs. The positions of the water oxygen atoms of the sI and sII clathrate hydrate phases were taken from X-ray crystallography and the water hydrogen atoms assigned to oxygen atoms in the unit cell in such a way as to simultaneously satisfy the ice rules and minimize the net unit cell dipole moment. The centers of mass of the guests are initially put in the center of the hydrate cages. Simulations cells of the sI clathrate hydrates use 3 × 3 × 3 replicas of the unit cell with 162 large cages and 54 small cages. Simulations of the sII clathrate hydrate use a 2 × 2 × 2 replica of the unit cell with 64 large cages and 128 small cages. The constant temperature−constant pressure simulations were carried out at 180, 200, 220, and 240 K.

In the simulations, the van der Waals and electrostatic intermolecular interactions of water are modeled with the TIP4P[12] and TIP4P/ice potential,[13] THF with the AMBER force field,[15] NH_3 with the OPLS force field of Rizzo and Jorgensen,[16] the TRAPPE potential for CH_4,[17] the NH_4^+ with the force field of Boudon and Wipff,[18] the OH^- ion with the force field of Zangi and Engerts,[19] and methanol with the van Leeuwen and Smit potential.[20] The potential parameters in the force fields are given in Table 1. The partial atomic electrostatic charges on THF are calculated using the CHELPG method, and the other guest molecules include partial atomic charges as part of the force field. Water and guest molecules are given freedom of motion in the simulations, but their internal structures are considered rigid. A cutoff of 1.3 nm is used for the long-range forces in the simulations.

Table 1. Atomic Point Charges and Lennard−Jones Parameters for H_2O, THF, CH_4, NH_3, NH_4^+, and OH^-

atom	q/e	σ_{ii}/nm	ε_{ii}/kJ·mol^{-1}
OW (H_2O, TIP4P)	0.0	0.3153	0.6485
HW (H_2O, TIP4P)	+0.5200	0.000	0.000
M (H_2O, TIP4P)	−1.0400	0.000	0.000
OW (H_2O, TIP4P/ice)	0.0	0.31668	0.8821
HW (H_2O, TIP4P/ice)	+0.5897	0.000	0.000
M (H_2O, TIP4P/ice)	−1.1794	0.000	0.000
C (CH_4)	0.0	0.3730	1.2305
CT (CH_3OH)	+0.265	0.3740	0.875
OH (CH_3OH)	−0.700	0.3030	0.719
HO (CH_3OH)	+0.435	0.0	0.0
Nh (NH_3)	−1.02	0.342	0.711
Hn (NH_3)	+0.34	0.0	0.0
Nh+ (NH_4^+)	−0.40	0.325	0.711
Hn+ (NH_4^+)	+0.35	0.0	0.0
Oh (OH^-)	−1.41	0.3166	0.6506
Ho (OH^-)	0.41	0	0.0

Simulations for each clathrate hydrate are performed in two stages. First a 600 ps constant pressure-constant temperature (NPT) simulation is performed, with 100 ps of temperature scaled equilibration to bring the clathrate hydrate with each guest combination to the desired pressure and temperature. To study the stability of the hydrate phases at the temperature of simulation, the 240 K runs were continued for a total simulation time of 1.5 ns. If the hydrate at 240 K showed signs of decomposition within this simulation time, the simulations at lower temperature were also continued for 1.5 ns or longer to determine whether the hydrates at the lower temperature also decompose. All simulations were performed at ambient pressure (0.1 MPa).

Simulations are performed on the (i) sI clathrate hydrates of CH_3OH and NH_3 in the large cages and empty small cages; (ii) sI clathrate hydrates of CH_3OH and NH_3 in the large cages and methane in the small cages; (iii) sII hydrates with THF in the large cages and CH_3OH/NH_3 in the small cages; and (iv) sI clathrate hydrates with NH_3 in the large cages and methane in the small cages with 11 of the 162 NH_3 molecules in the large cages replaced by NH_4^+ guest molecules. This mimics the effect of proton transfer from the lattice water molecules to the basic ammonia guests. For charge neutrality, a water molecule from each large cage holding a NH_4^+ guest is replaced by an OH^- group at the same lattice position.

The hydrogen bonding of the THF, NH_3, CH_3OH, and NH_4^+ guests with the lattice water molecules are studied. For NH_3 and CH_3OH guests, we consider both proton-donating and proton-accepting hydrogen bonding with the water molecules of the hydrate framework. Hydrogen bonds are determined from peaks in the radial distribution functions (RDFs) at distances near 0.2 nm. These peaks at each

dx.doi.org/10.1021/je5006517 | J. Chem. Eng. Data 2015, 60, 389−397

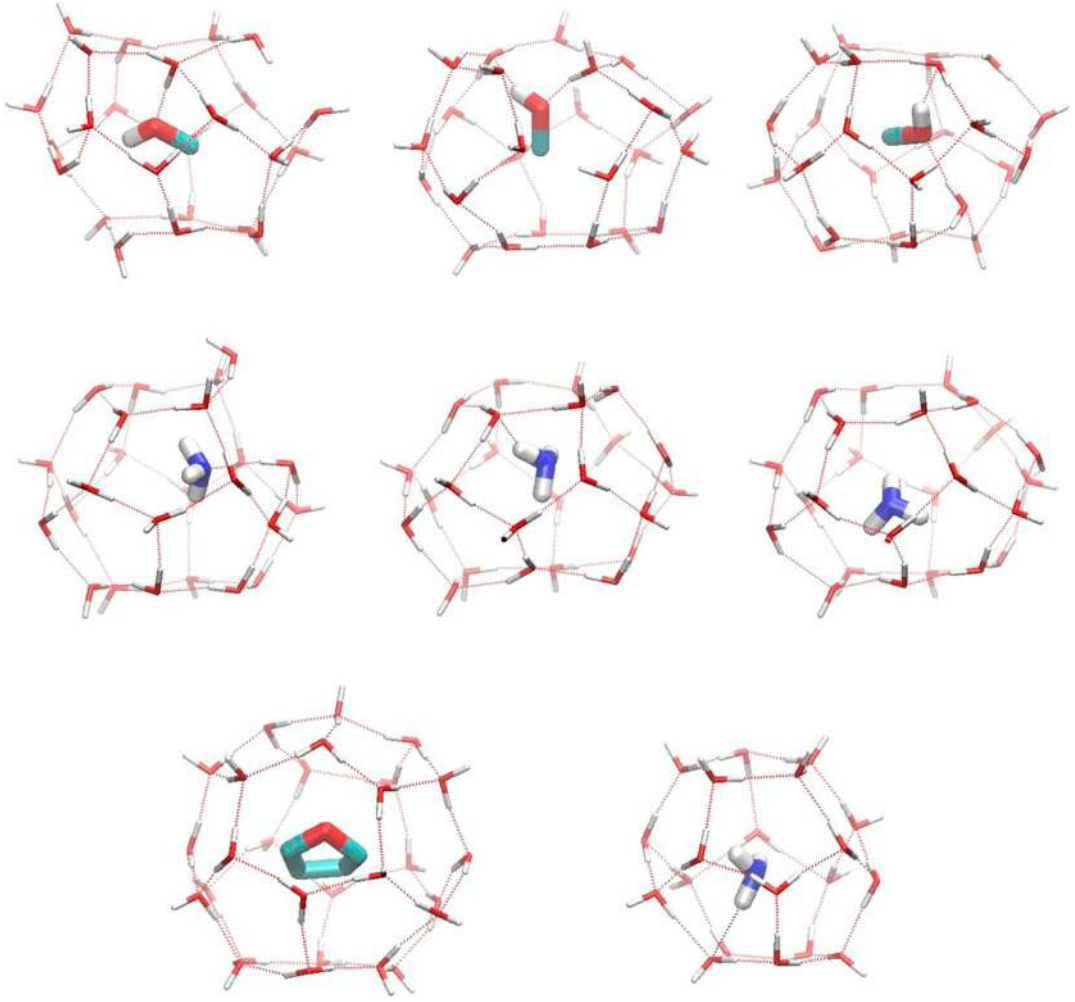

Figure 1. Snapshots extracted from the periodic clathrate hydrate simulation cell trajectory showing hydrogen bonding guests and their surrounding cages. Simulations are at 240 K using the TIP4P/ice water potential. The top row shows configurations of methanol in the large cages from the sI CH_3OH + CH_4 simulation, the middle row shows configurations of ammonia from the sI NH_3 + CH_4 simulation, and the bottom row shows a configuration of THF in the large cage and ammonia in a small cage from the sII THF + NH_3 simulation.

temperature are related to the ensemble average number of hydrogen bonds $\langle P(T)\rangle$ by

$$\langle P(T)\rangle = \int_0^{r_{min}} \rho g(r) 4\pi r^2 \, dr \quad (1)$$

In eq 1, r_{min} is the first minimum in the RDF which appears after the hydrogen bond peak at ~0.2 nm.

To compare the stability of the NH_3 and CH_3OH guests in the sI cages with the CH_4 in these cages, we performed thermodynamic integration calculations to determine the free energy of substituting methane in the large sI cages with NH_3 and CH_3OH guests. The Gibbs free energy associated with the methane guest substitution reaction,

$$\text{clathrate}[(n + x)CH_4] + xX(g) \rightarrow \text{clathrate}[nCH_4 + xX] + xCH_4(g) \quad (2)$$

is calculated, where x molecules of NH_3 or CH_3OH (considered as hypothetical ideal gas molecules) at a temperature T and pressure p confined to the volume of the clathrate hydrate simulation cell replace xCH_4 molecules from the large cages of the sI clathrate hydrate. The $CH_4(g)$ molecules released from the product are noninteracting ideal gas molecules confined to the simulation cell. We focus on comparing the stability of the methane/ammonia/methanol guests in the cages and do not consider free energy contributions from nonideality effects in the gas or liquid phase. Further details of the procedure for calculating the free energy of substitution are in ref 21. Performing free energy calculation in this manner emphasizes the relative stability of the guest species in the clathrate hydrate cages. The free energies associated with eq 2 are calculated using the thermodynamic integration (TI) technique with nonlinear scaling of the intermolecular interaction potentials.[22]

To study the effect of the water force field on the hydrogen bonding of the water with the guest molecules, we did simulations with the TIP4P and TIP4P/ice potentials. The TIP4P/ice potential predicts a more accurate value for the decomposition temperature of methane hydrate and also gives better predictions of lattice constants compared to the TIP4P potential.[23] However, the TIP4P potential is widely used in hydrate simulations and comparing the effect of the two potentials on the hydrogen bonding probabilities would be of interest.

dx.doi.org/10.1021/je5006517 | J. Chem. Eng. Data 2015, 60, 389−397

RESULTS AND DISCUSSION

Snapshots of cages isolated from the simulation cell for several of the simulations are shown in Figure 1. Trajectory data to view animations of the hydrogen bonding guest molecules and their surrounding cage of water molecules are given in the Supporting Information. Proton-donating and proton-accepting hydrogen bonds with the water molecule are observed with the methanol hydroxyl group and ammonia.

The presence of hydrogen bonding of the guests with the hydrate framework water is determined by plotting the RDFs of the guests with water. The RDFs for the sI CH_3OH + CH_4 and sI NH_3 + CH_4 hydrates are shown in Figure 2, and those of the

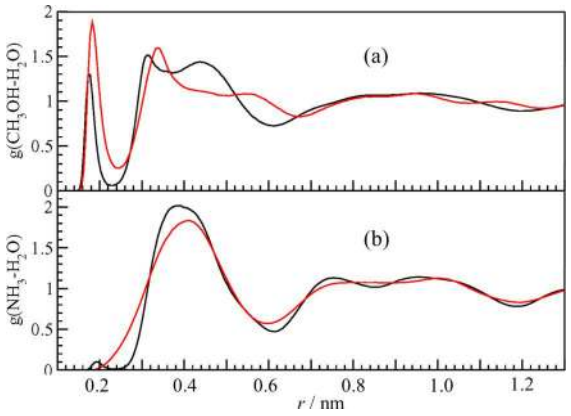

Figure 2. Radial distribution functions at 240 K using the TIP4P/ice potential for (a) the sI CH_3OH (L) + CH_4(S) clathrate hydrate. Guest $CH_3(H)O\cdots HOH$ (black curve) and $CH_3OH\cdots OH_2$ (red curve) spatial correlations are both shown. (b) The sI NH_3 (L) + CH_4 (S) clathrate hydrate. Guest $H_3N\cdots HOH$ (black curve) and $H_2N{-}H\cdots OH_2$ (red curve) spatial correlations are both shown. Hydrogen-bonding interactions are characterized by peaks in the RDFs near 0.2 nm. See text for discussion.

sII hydrates of THF + CH_3OH and THF + NH_3 are shown in Figure 3. These RDFs are from simulations at 240 K using the

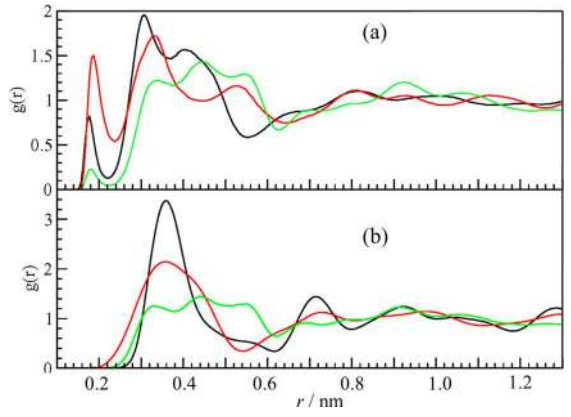

Figure 3. Radial distribution functions at 240 K using the TIP4P/ice potential for (a) the sII THF (L) + CH_3OH (S) clathrate hydrate. Guest $CH_3(H)O\cdots HOH$ (black curve), $CH_3OH\cdots OH_2$ (red curve), and $(CH_2)_4O\cdots HOH$ (green curve) spatial correlations are shown. (b) The sII THF (L) + NH_3 (S) clathrate hydrate. Guest $H_3N\cdots HOH$ (black curve), and $H_2N{-}H\cdots OH_2$ (red curve), and $(CH_2)_4O\cdots HOH$ (green curve) spatial correlations are shown. Hydrogen-bonding interactions are characterized by peaks in the RDFs near 0.2 nm. See text for discussion.

TIP4P/ice potential. The presence of hydrogen bonds is shown by peaks in the RDFs of Figures 2 and 3 at the distance of about 0.2 nm.

In the sI clathrate hydrates with the TIP4P/ice potential for water shown in Figure 2, methanol forms proton-donating and accepting hydrogen bonds with water. Ammonia shows a weaker proton-accepting hydrogen bond ($H_3N\cdots HOH$) and spatially diffuse proton-donating hydrogen bonding ($H_2N{-}H\cdots OH_2$). In the sII binary THF clathrate hydrates simulations with the TIP4P/ice potential shown in Figure 3, methanol in the small cages shows proton-donating and accepting hydrogen bonding with water. Ammonia shows no proton-accepting hydrogen bond ($H_3N\cdots HOH$) and spatially diffuse proton-donating hydrogen bonding. The THF hydrogen bond peak with water is discernible in the THF + CH_3OH clathrate hydrate but is not observed in the binary hydrate with ammonia.

Similar RDF curves for the TIP4P potential at 240 K are given in Figure 4. In the case of the simulations with the TIP4P

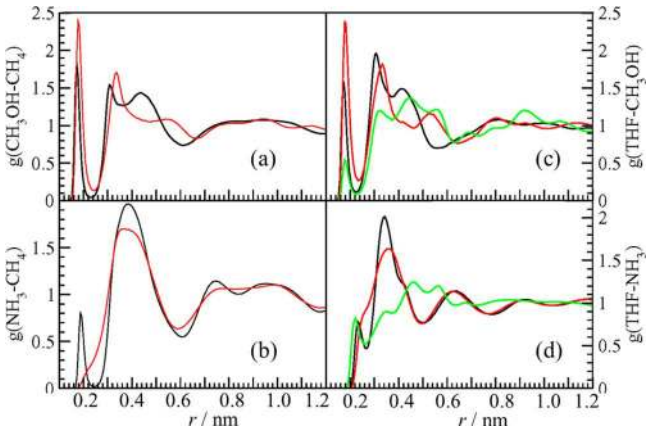

Figure 4. Radial distribution functions at 240 K using the TIP4P potential for (a) the sI CH_3OH (L) + CH_4 (S) clathrate hydrate. Guest $CH_3(H)O\cdots HOH$ (black curve) and $CH_3OH\cdots OH_2$ (red curve) spatial correlations are shown. (b) The sI NH_3 (L) + CH_4 (S) clathrate hydrate. Guest $H_3N\cdots HOH$ (black curve) and $H_2N{-}H\cdots OH_2$ (red curve) spatial correlations are shown. (c) The sII THF (L) + CH_3OH (S) clathrate hydrate. Guest $CH_3(H)O\cdots HOH$ (black curve), $CH_3OH\cdots OH_2$ (red curve), and $(CH_2)_4O\cdots HOH$ (green curve) spatial correlations are shown. (d) The sII THF (L) + NH_3 (S) clathrate hydrate. Guest $H_3N\cdots HOH$ (black curve), $H_2N{-}H\cdots OH_2$ (red curve), and $(CH_2)_4O\cdots HOH$ (green curve) spatial correlations are shown.

potential, the extent of hydrogen bonding is larger for both methanol and (particularly for) ammonia. The pure sI NH_3 hydrate and binary sI NH_3 (L) + CH_4 (S) hydrate decompose in the simulations at 220 K and 240 K, respectively. The large change in hydrogen bonding probability with the change in the water force field, shown in Table 1, is notable and is discussed further below.

The average hydrogen bonding number $\langle P(T)\rangle$ from eq 1 at different temperatures for the NH_3, CH_3OH, and THF guests in the different pure and mixed sI and sII hydrates studied in this work are given in Tables 2 and 3 for simulations with the TIP4P/ice and TIP4P water potentials, respectively. In all cases, there is a greater probability of hydrogen bonding between methanol and ammonia with water in simulations with the TIP4P potential compared with simulations using the TIP4P/ice potential. The TIP4P/ice model has stronger

dx.doi.org/10.1021/je5006517 | J. Chem. Eng. Data 2015, 60, 389−397

Table 2. Average Number of Hydrogen Bonds for the CH_3OH, NH_3 and THF with Water in Hydrates at Different Temperatures from Simulations Using the TIP4P/Ice Potential for Water[a]

hydrogen bonding guest [hydrate phase]	temperature/K 180	200	220	240
sI: NH_3 (L)	0.011	0.028	0.046	0.076
sI: [NH_3 (L) + CH_4 (S)]	0.021	0.019	0.031	0.083
sI: CH_3OH (L)	0.844, 0.947	0.844, 0.925	0.865, 0.918	0.887, 0.900
sI: [CH_3OH (L) + CH_4 (S)]	0.796, 0.942	0.814, 0.921	0.809, 0.901	0.806, 0.858
sII: NH_3 (S) [+ THF (L)]	0.007	0.002	0.004	0.010
sII: THF (L) [+ NH_3 (S)]	>0.001	>0.001	>0.001	>0.001
sII: CH_3OH (S) [+ THF (L)]	0.674, 0.936	0.619, 0.890	0.568, 0.851	0.548, 0.773
sII: THF (L) [+ CH_3OH (S)]	0.207	0.192	0.163	0.176

[a]In cases where two numbers are given, the first is for proton-accepting hydrogen bonds with HW, and the second is for hydrogen bonds with OW.

Table 3. Average Number of Hydrogen Bonds for the CH_3OH, NH_3, and THF with Water in Hydrates at Different Temperatures from Simulations Using the TIP4P Potential for Water[a]

hydrogen bonding guest [hydrate phase]	temperature/K 180	200	220	240
sI: NH_3 (L)	0.448	0.659		
sI: NH_3 (L+S)[a]	0.738; 0.575	0.864; 0.790		
sI: [NH_3 (L) + CH_4 (S)]	0.404	0.581	0.777	
sI: CH_3OH (L)[b]	1.059; 0.956	1.068; 0.959	1.144; 0.950	
sI: CH_3OH (L+S)[c]	1.08;1.14	1.10;1.23	1.23;1.32	1.35; 1.38
sI: [CH_3OH (L) + CH_4 (S)][b]	1.030; 0.956	1.039; 0.935	1.048; 0.927	1.109; 0.932
sII: NH_3 (S) [+ THF (L)]	0.085	0.150	0.239	0.330
sII: THF (L) [+ NH_3 (S)]	>0.001	0.015	0.043	0.091
sII: CH_3OH (S) [+ THF (L)][b]	0.960; 0.974	0.961; 0.959	0.984; 0.932	1.028; 0.911
sII: THF (L) [+ CH_3OH (S)]	0.411	0.413	0.457	0.479

[a]The first number is the $H_3N\cdots HOH$ bond in the large cages, and the second number is the $H_3N\cdots HOH$ bond in the small cages. [b]The first number is the $CH_3(H)O\cdots HOH$ bond, and the second number is the $CH_3OH\cdots OH_2$ bond. [c]The first number is the $CH_3(H)O\cdots HOH$ bond in the large cages, and the second number is the same hydrogen bond in the small cages. [a]In cases where two numbers are given, the first is for proton-accepting hydrogen bonds with HW, and the second is for hydrogen bonds with OW.

water−water van der Waals and electrostatic interaction potentials, and it is not surprising that this potential leads to a lesser degree of hydrogen bonding than the TIP4P potential. It is known that the TIP4P/ice potential predicts better ice phase diagram than the TIP4P potential,[8] and the three-phase equilibrium line for methane gas−hydrate−water system is more accurate for the TIP4P/ice potential than TIP4P which predicts an equilibrium line which is between 30 K and 40 K too low at different pressures.[23]

The results in Tables 2 and 3 show that methanol consistently has a higher hydrogen bonding probability with the cage water molecules than ammonia. The physical origin for this can be determined by comparing the force field parameters for these two molecules in Table 1. The nitrogen of ammonia actually has a larger electrostatic charge ($-1.02e$) than the oxygen of methanol ($-0.700e$), but ammonia nitrogen has a smaller probability of forming proton-accepting hydrogen bonds than the methanol oxygen. The driver of hydrogen bonding for methanol may be the larger size of this molecule as a result of the presence of the methanol $-CH_3$ group and not electrostatic attraction. The larger size of methanol pushes the −OH group closer to the cage wall and enhances the hydrogen-bonding probability.

Another consequence of the different water potential models is the lower decomposition temperatures for the ammonia hydrates predicted by the TIP4P simulations as compared to the TIP4P/ice simulations. The effect of ammonia−water hydrogen bonding between the TIP4P/ice and TIP4P simulations is particularly striking in hydrates where the large degree of $H_3N\cdots HOH$ hydrogen bonding in the TIP4P simulations has led to destabilization of the sI ammonia containing clathrate hydrates; see Table 3. Despite the stronger hydrogen bonding of CH_3OH with the cage waters in both the TIP4P/ice and TIP4P potentials, the hydrophobic CH_3 group of methanol stabilizes the hydrates under simulation conditions that lead to the decomposition of the analogous ammonia hydrates.

In the sI hydrates, the degree of ammonia and methanol proton-accepting hydrogen bonds, i.e., $H_3N\cdots HOH$ and $CH_3(H)O\cdots HOH$, respectively, increase with temperature for both TIP4P/ice and TIP4P potentials, but the extent of proton-donating hydrogen bonds, i.e., $H_2N-H\cdots OH_2$ and $CH_3OH\cdots OH_2$, decreases with temperature. The trends in hydrogen bonding for methanol, ammonia, and THF in the sII binary hydrates with THF are more complex and differ between the two water potential simulations.

An interesting aspect observed in the ammonia and methanol simulations is that these guests can displace a water molecule and become incorporated into the water lattice; see Figure 5. The displacement of water from the lattice site by one of these guests creates Bjerrum defects in the lattice which can enhance the diffusion of species through the hydrate phase. The displacement of water by ammonia occurs more frequently than the displacement of water by methanol. The reason for this can be that ammonia is isoelectronic with water and can form four hydrogen bonds with the other water molecules in the hydrate lattice (albeit, leading to the formation of Bjerrum D-defects). Methanol, on the other hand, has a large methyl group and can only form three hydrogen bonds with neighboring water molecules.

The water molecules displaced by ammonia are pushed into neighboring small or large clathrate hydrate cages which can already be occupied by other guests. The displaced and encaged water can itself form hydrogen bonds with its new cage or coguest. Water guests have previously been observed in clathrate hydrate cages.[24−26] The cage where the ammonia (now in the water lattice) originated becomes empty. As the sII clathrate hydrate phase has some tolerance for empty small cages, this should not drastically affect the stability of the hydrate phase. Simulations show that the caged water

dx.doi.org/10.1021/je5006517 | J. Chem. Eng. Data 2015, 60, 389−397

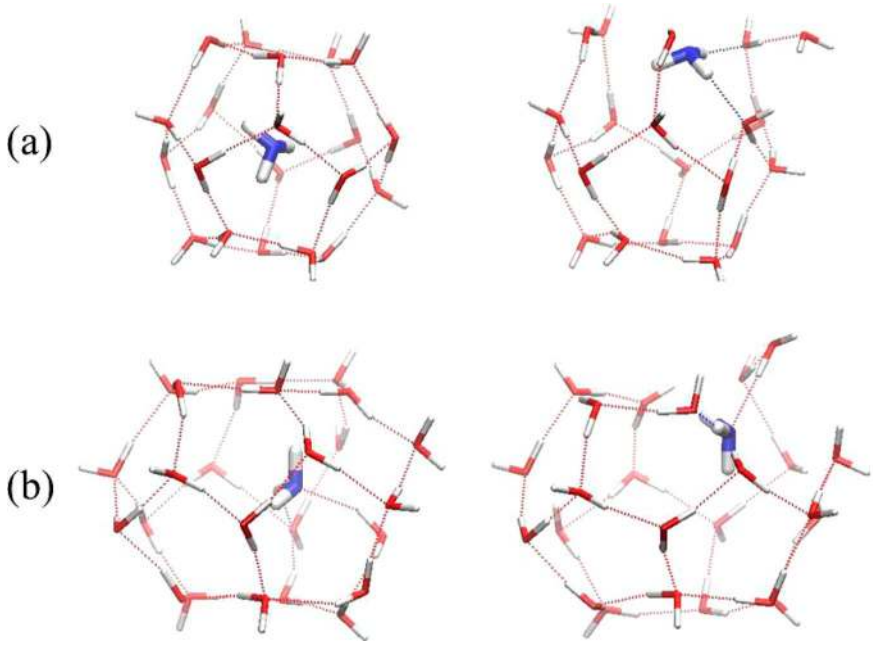

Figure 5. Ammonia guests in the small cages (a) and large cages (b) of the sI clathrate hydrate can move into a water lattice site and displace a water molecule for a span of time. On the left, configurations with the ammonia molecules inside the cages are shown, and on the right configurations with the ammonia displace a cage water molecule are shown.

molecules are quite mobile and diffuse through neighboring cages.[26]

Ammonia is a base, and there is some probability for proton transfer from water to ammonia to produce NH_4^+ ions in the clathrate hydrate cages with the formation of an equivalent number of OH^- groups. We consider a sI NH_3 + CH_4 hydrate where 11 of the 162 ammonia molecules in the large cages have been converted to NH_4^+. In simulations using the TIP4P/ice potential, this sI clathrate hydrate was found to be stable in the same temperature range as the binary NH_3 + CH_4 hydrate without proton transfer.

In addition to its larger size, the NH_4^+ guest remains associated with the lattice OH^- due to strong electrostatic interactions between these two ions. A snapshot of three large sI cages, one of which holds a NH_4^+ guest, is shown in Figure 6a and the Cartesian coordinates of the atoms for this sample configuration are provided in the Supporting Information. Two of the cages shown on the left have hexagonal faces perpendicular to the simulation *y*-axis, and the cage on the right-hand side has hexagonal faces perpendicular to the simulation *x*-axis. The NH_4^+ is tethered to the OH^- group in the large cage lattice for the duration of the simulation trajectory. A water molecule (shown by the dashed circle) deviates significantly from its lattice position to hydrogen bond with the NH_4^+ guest. Significant defects are introduced in the hydrate structure in the region near the NH_4^+ guest.

A view of the cages showing the vicinity of the OH^- group is shown in Figure 6b. Neighboring water molecules in the cage lattice form four proton-donating hydrogen bonds with the OH^- group, leading to the formation of Bjerrum L-defects and large distortions in the hydrate lattice. Despite these large lattice distortions, the clathrate hydrate can tolerate a limited number of the NH_4^+ ions as guests in the lattice.

The radial distribution functions for the NH_4^+ and OH^- ions are given in Figure 7. The top panel shows the $H_3N\cdots HOH$ RDF, which is similar to that of the sI NH_3 + CH_4 hydrate shown in Figure 2. The middle panel shows the $[H_3N{-}H]^+\cdots OH^-$ RDF (black curve) and the $[H_3N{-}H]^+\cdots OH_2$ RDF (red curve). The NH_4^+ and OH^- ions interact strongly and at the same time the NH_4^+ ions strongly hydrogen bond with water molecules in the lattice at distances less than 0.2 nm. The bottom panel shows the RDF for the strong $HO{-}H\cdots OH^-$ hydrogen bonds (black curve) which have a peak at a distance less than 0.2 nm. This interaction leads to the formation of Bjerrum L-defects. Also shown in the bottom panel is the RDF of the $H_2O\cdots H{-}O^-$ hydrogen bonds, which are much weaker. As seen in Figure 6, the O−H bond of the hydroxyl group points toward the center of a cage and does not directly hydrogen bond with lattice water molecules.

The different dynamics of the NH_3 and NH_4^+ guests in the large sI cages are shown by the reduced velocity autocorrelation function $\mathrm{VACF}(t) = \langle \mathbf{v}(t)\cdot\mathbf{v}(0)\rangle/\langle \mathbf{v}(0)\cdot\mathbf{v}(0)\rangle$ of the corresponding nitrogen atoms at 240 K in Figure 8. The NH_3 molecules show low hydrogen bonding probability with cage water molecules (see Table 2) and have relatively free rattling motion in the large sI cages with a period of ∼1 ps. The NH_4^+ guests, on the other hand, are tethered to the OH^- group and undergo mostly short-range vibrational motions in the cages with much smaller periods.

The lattice constants predicted by the TIP4P/ice and TIP4P potentials for the sI and sII clathrate hydrates are given in Tables 4 and 5, respectively, and plotted in Figures 9 and 10. In all cases, the hydrates with NH_3 have smaller lattice constants than the analogous hydrates with CH_3OH. This was experimentally observed in our recent work.[27] Adding methane to empty small cages of the sI hydrates increases the lattice constant. However, the clathrate hydrates with methane in the small cages have smaller lattice constants than analogous clathrate hydrates with NH_3 or CH_3OH in the small cages. The predicted lattice constants are generally smaller, but the thermal expansivities predicted for the clathrate hydrates with the

dx.doi.org/10.1021/je5006517 | J. Chem. Eng. Data 2015, 60, 389−397

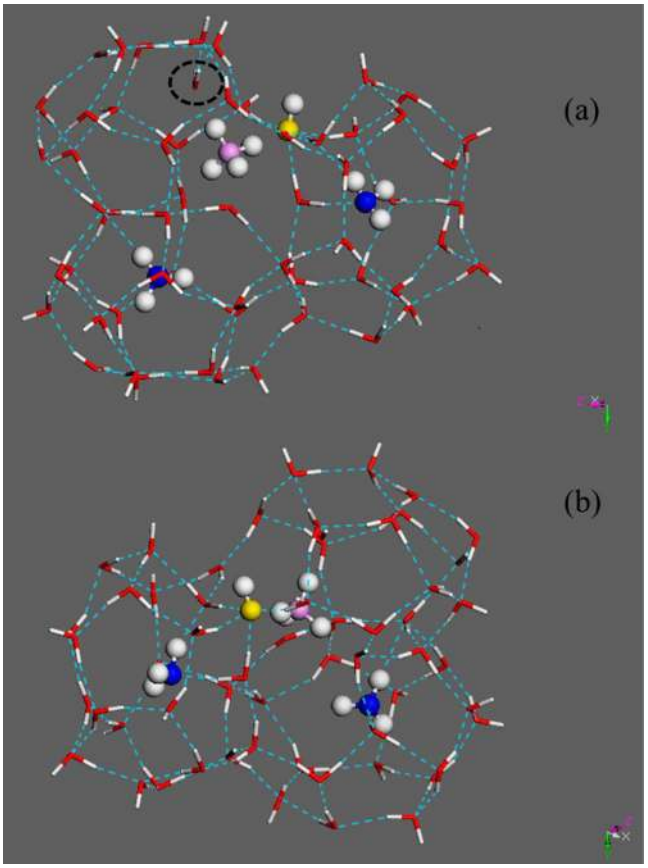

Figure 6. (a) Snapshot of a cage with NH_4^+ as a guest and an OH^- in the cage lattice. The distortion of the lattice in the vicinity of the NH_4^+ and OH^- groups is clear. A water molecule which has moved out of its lattice position and entered the cage to interact with the NH_4^+ is shown with the dashed circle. The water oxygen atoms are shown in red, hydrogen atoms are shown in white, ammonia nitrogen atoms are shown in blue, the ammonium nitrogen atom is shown in lavender, and the hydroxyl oxygen atom is shown in yellow color. (b) The four water proton-donating hydrogen bonds to the hydroxyl oxygen can be seen in this view.

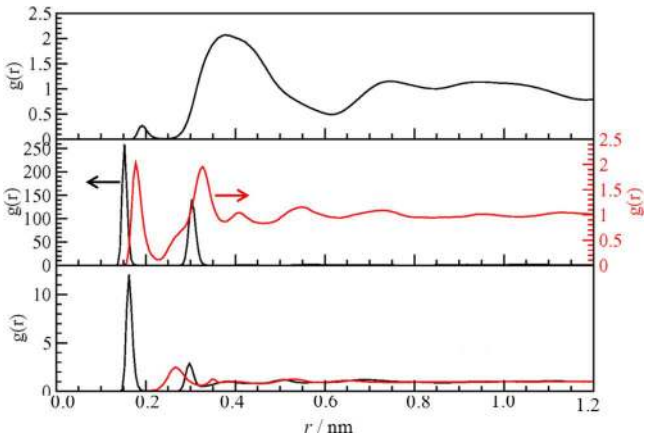

Figure 7. Radial distribution functions at 180 K for the simulation of the sI NH_3 + NH_4OH + CH_4 phase. Top panel, the $H_3N\cdots HOH$ RDF. Middle panel, $H_3N^+H\cdots OH^-$ (black curve) and $H_3N^+H\cdots OH_2$ (red curve) RDFs. Bottom panel, $HO^-\cdots HOH$ (black curve) and $^-OH\cdots OH_2$ (red curve) RDF. See text for discussion.

TIP4P potential are generally larger than that of the TIP4P/ice potential.

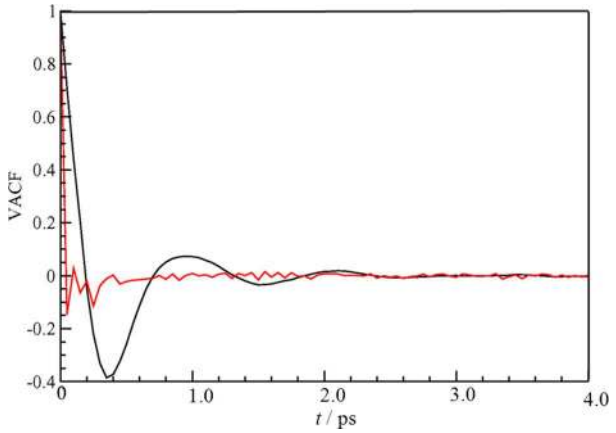

Figure 8. Velocity autocorrelation function for the NH_3 (black line) and NH_4^+ (red line) guests at 240 K.

Table 4. Lattice Constant (nm) for the sI and sII Hydrates Containing CH_3OH and NH_3 at Different Temperatures from Simulations Using the TIP4P/Ice Potential for Water

hydrogen bonding guest [hydrate phase]	temperature/K			
	180	200	220	240
sI: NH_3 (L)	1.19188	1.19347	1.19504	1.19688
sI: [NH_3 (L) + CH_4 (S)]	1.19309	1.19468	1.19641	1.19870
sI: [NH_3 (L) + 10% NH_4OH (L) + CH_4 (s)]	1.19216	1.19468	1.19571	1.19844
sI: CH_3OH (L)	1.19966	1.20169	1.20288	1.20450
sI: [CH_3OH (L) + CH_4 (S)]	1.20115	1.20330	1.20482	1.20677
sII: [THF (L) + NH_3 (S)]	1.72238	1.72495	1.72773	1.73064
sII: [THF (L) + CH_3OH (S)]	1.73450	1.73790	1.74086	1.74436

Table 5. Lattice Constant (nm) for the sI and sII Hydrates Containing CH_3OH and NH_3 at Different Temperatures from Simulations Using the TIP4P Potential for Water

hydrogen bonding guest [hydrate phase]	temperature/K			
	180	200	220	240
sI: NH_3 (L)	1.18110	1.18533		
sI: NH_3 (L+S)	1.18788	1.19538		
sI: [NH_3 (L) + CH_4 (S)]	1.18184	1.18640	1.19183	
sI: CH_3OH (L)	1.18984	1.19145	1.19368	
sI: CH_3OH (L+S)	1.19600	1.19964	1.20970	1.22242
sI: [CH_3OH (L) + CH_4 (S)]	1.19109	1.19387	1.19677	1.20014
sII: [THF (L) + NH_3(S)]	1.70906	1.71404	1.72005	1.72640
sII: [THF (L) + CH_3OH (S)]	1.73003	1.73560	1.74129	1.74801
sII: [NH_3 (L+S)]	1.72004	1.72386		

The free energies of eq 2, for substitution of CH_4 in cages of sI methane hydrate by NH_3 and CH_3OH, are calculated using the TIP4P potential. The free energies per CH_4/NH_3 substitution at 200 K are -1.9 kJ·mol^{-1} and -1.4 kJ·mol^{-1} for the substitution in the large and small cages, respectively. The free energies per CH_4/CH_3OH substitution at 200 K are -3.7 kJ·mol^{-1} for the substitution in the large cages. These results show that the NH_3 and CH_3OH are more stable in the hydrate large cages that CH_4. The data used for λ-integration in

dx.doi.org/10.1021/je5006517 | J. Chem. Eng. Data 2015, 60, 389−397

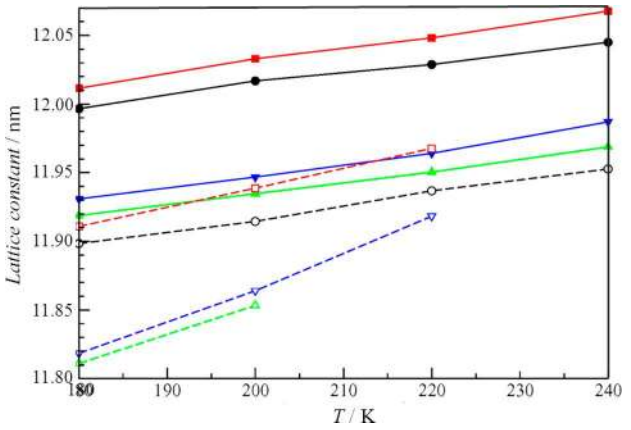

Figure 9. Variation of lattice constants for selected sI clathrate hydrates of methanol and ammonia at different temperatures using the TIP4P/ice and TIP4P potentials. The TIP4P/ice potential predicts larger lattice constants and a smaller thermal expansivity for the lattice. The force field and hydrate as specified as ●, TIP4P/ice CH_3OH (L); red ■, TIP4P/ice CH_3OH (L) + CH_4 (S); green ▲, TIP4P/ice NH_3 (L); blue ▼, TIP4P/ice NH_3 (L) + CH_4 (S); ○, TIP4P CH_3OH (L); red □, TIP4P CH_3OH (L) + CH_4 (S); green △, TIP4P NH_3 (L); blue ▽, TIP4P NH_3 (L) + CH_4 (S).

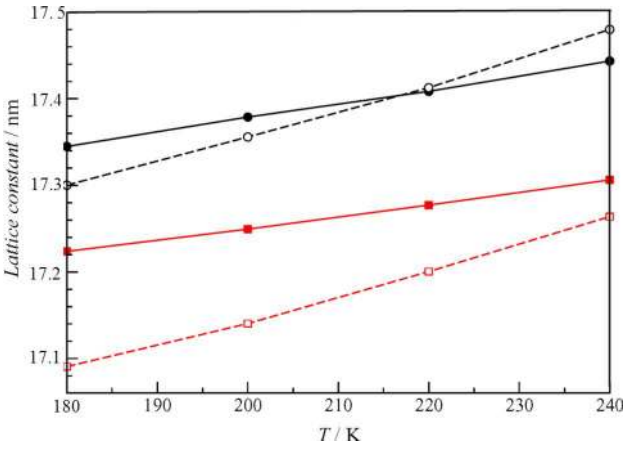

Figure 10. Lattice constants for selected sII binary THF clathrate hydrates of methanol and ammonia at different temperatures using the TIP4P/ice and TIP4P potentials. The TIP4P/ice potential predicts larger lattice constants and a smaller thermal expansivity for the lattice. The force field and hydrate as specified as ●, TIP4P/ice THF (L) + CH_3OH (S); red ■, TIP4P/ice THF (L) + NH_3 (S); ○, TIP4P THF (L) + CH_3OH (S); red □, TIP4P THF (L) + NH_3 (S).

the thermodynamic integration procedure are given in Figures S1 and S2 in the Supporting Information.

CONCLUSIONS

We have simulated methanol and ammonia in sI and sII clathrate hydrates with the TIP4P/ice and TIP4P water potentials and existing force fields for the various guest molecules. Methanol and ammonia both form hydrogen bonds with lattice water with CH_3OH showing a higher probability for hydrogen bonding in each analogous structure; see Tables 2 and 3. Despite this observation, in the TIP4P potential simulations, the ammonia-containing hydrates decompose at lower temperatures than the CH_3OH containing analogues. This could be due to the steric effect of the hydrophobic CH_3 group of methanol which stabilizes the water cages. Methanol forms both proton-donating and proton-accepting hydrogen bonds with water, whereas ammonia mostly forms proton-accepting hydrogen bonds. The ammonia proton-donating hydrogen bonds, $H_2N{-}H{\cdots}OH_2$, are more diffuse and in many cases, particularly in the TIP4P/ice potential simulations, do not show up as a sharp peak in the RDF.

The free energies associated with methane guest substitution in the clathrate hydrate cages with ammonia or methanol are negative. The reason these substances act as thermodynamic clathrate hydrate inhibitors for the formation of methane hydrate may be associated with the free energy penalty of removal of the polar NH_3 or CH_3OH molecules from the nonideal gas or aqueous solution phase.

The effect of the water and guest molecule force fields on the decomposition temperature of methane hydrate has been studied. In this work, we observe that the choice of water force field has a substantial quantitative effect on the hydrogen bonding of guests with water in various clathrate hydrates. Experimental observations show that the THF + CH_3OH and THF + NH_3 clathrate hydrates are at least stable up to the 233 K and 263 K, respectively.[9,10] The stability of the THF + CH_3OH and THF + NH_3 simulations at 263 K for both the TIP4P/ice and TIP4P potentials are consistent with these experimental results. A recent experimental work states that the THF clathrate hydrates synthesized in the presence of NH_3 in concentrations ranging from 0 to 0.25 mass fraction begin to decompose at 203.6 K.[28] Further study is need to determine if the exact conditions of the THF binary hydrate decomposition and how these experimental results can be used to distinguish between the predictions of the different force fields used in the simulation.

ASSOCIATED CONTENT

Supporting Information

Two files giving the trajectory data (time dependence of Cartesian coordinates) for the motion of CH_3OH and NH_3 guests in the large sI clathrate hydrate cages. A set of Cartesian coordinates for a fragment of clathrate hydrate structure in the vicinity of the NH_4^+ guest in the sI NH_3 + NH_4OH + CH_4 clathrate hydrate. Two figures showing the data used for thermodynamic integration. This material is available free of charge via the Internet at http://pubs.acs.org.

AUTHOR INFORMATION

Corresponding Authors

*E-mail: saman.alavi@nrc-cnrc.gc.ca.

*E-mail: john.ripmeester@nrc-cnrc.gc.ca.

Funding

The support of the National Research Council of Canada is acknowledged.

Notes

The authors declare no competing financial interest.

REFERENCES

(1) Davison, D. W. Clathrate Hydrates. In *Water: A Comprehensive Treatise*; Franks, F., Ed.; Plenum Press: New York, 1973; Vol. 2, p 115.

(2) Jeffrey, G. A. Hydrate Inclusion Compounds. In *Comprehensive Supramolecular Chemistry*; Atwood, J. L., Davies, J. E. D., MacNicol, D. D., Vogtle, F., Eds.; Pergamon: Oxford, U.K., 1996; Vol. 6, p 757.

(3) Alavi, S.; Udachin, K. A.; Ratcliffe, C. I.; Ripmeester, J. A. Clathrate Hydrates. In *Supramolecular Chemistry: From Molecules to Nanomaterials*; Wiley: Chichester, UK, 2011.

(4) Alavi, S.; Susilo, R.; Ripmeester, J. A. Linking microscopic guest properties to macroscopic observables in clathrate hydrates: Guest-host hydrogen bonding. *J. Chem. Phys.* **2009**, *130*, 174501.
(5) Alavi, S.; Udachin, K. A.; Ripmeester, J. A. Effect of guest-host hydrogen bonding on the structures and properties of clathrate hydrates. *Chem.—Eur. J.* **2010**, *16*, 1017−1025.
(6) Buch, V.; Devlin, J. P.; Monreal, I. A.; Jagoda-Cwiklik, B.; Aytemiz-Uras, N.; Cwiklik, L. Clathrate hydrates with hydrogen-bonding guests. *Phys. Chem. Chem. Phys.* **2009**, *11*, 10245−10265.
(7) Monreal, I. A.; Cwiklik, L.; Jagoda-Cwiklik, B.; Devlin, J. P. Classical to nonclassical transition of ether-HCN clathrate hydrates at low temperature. *J. Phys. Chem. Lett.* **2010**, *1*, 290−294.
(8) Sloan, E. D., Jr.; Koh, C. A. *Clathrate Hydrates of Natural Gases*, 3rd ed.; CRC Press: Boca Raton, FL, 2008.
(9) Shin, K.; Kumar, R.; Udachin, K. A.; Alavi, S.; Ripmeester, J. A. Ammonia clathrate hydrates as new solid phases for Titan, Enceladus, and other planetary systems. *Proc. Natl. Acad. Sci. U.S.A.* **2012**, *109*, 14785−14790.
(10) Shin, K.; Udachin, K. A.; Moudrakovski, I. L.; Leek, D. M.; Alavi, S.; Ratcliffe, C. I.; Ripmeester, J. A. Methanol incorporation in clathrate hydrates and the implications for oil and gas pipeline flow assurance and icy planetary bodies. *Proc. Natl. Acad. Sci. U.S.A.* **2013**, *110*, 8437−8442.
(11) Shin, K.; Moudrakovski, I. L.; Davari, M. D.; Alavi, S.; Ratcliffe, C. I.; Ripmeester, J. A. Crystal engineering the clathrate hydrate lattice with NH_4F. *CrystEngComm* **2014**, *16*, 7209−7217.
(12) Jorgensen, W. L.; Chandrasekhar, J.; Madura, J. D.; Impey, R. W.; Klein, M. L. Comparison of Simple Potential Functions for Simulating Liquid Water. *J. Chem. Phys.* **1983**, *79*, 926−935.
(13) Abascal, J. L. F.; Sanz, E.; Garcia Fernandez, R.; Vega, C. A potential model for the study of ices and amorphous water: TIP4P/Ice. *J. Chem. Phys.* **2005**, *122*, 234511.
(14) Smith, W.; Forester, T. R.; Todorov, I. T. *DL_POLY 2 User Manual*, Version 2.20; Daresbury Lab: Daresbury, U.K., 2009.
(15) Cornell, W. D.; Cieplak, P.; Bayly, C. L.; Gould, I. R.; Merz, K. M., Jr.; Ferguson, D. M.; Spellmeyer, D. C.; Fox, T.; Caldwell, J. W.; Kollman, P. A. A Second Generation Force Field for the Simulation of Proteins, Nucleic Acids, and Organic Molecules. *J. Am. Chem. Soc.* **1995**, *117*, 5179−5197.
(16) Rizzo, R. C.; Jorgensen, W. L. OPLS All-Atom Model for Amines: Resolution of the Amine Hydration Problem. *J. Am. Chem. Soc.* **1999**, *121*, 4827−4836.
(17) Martin, M. G.; Siepmann, J. I. Transferable Potentials for Phase Equilibria. 1. United-Atom Description of *n*-Alkanes. *J. Phys. Chem. B* **1998**, *102*, 2569−2577.
(18) Boudon, S.; Wipff, G. Free energy calculations involving NH_4^+ in water. *J. Comput. Chem.* **1991**, *12*, 42−51.
(19) Zangi, R.; Engerts, J. B. F. N. Physisorption of Hydroxide Ions from Aqueous Solution to a Hydrophobic Surface. *J. Am. Chem. Soc.* **2005**, *127*, 2272−2276.
(20) van Leeuwen, M.; Smit, B. Molecular Simulation of the Vapor-Liquid Coexistence Curve of Methanol. *J. Phys. Chem.* **1995**, *99*, 1831−1833.
(21) Nohra, M.; Woo, T. K.; Alavi, S.; Ripmeester, J. A. Molecular dynamics Gibbs free energy calculations for CO_2 capture and storage in structure I clathrate hydrates in the presence of SO_2, CH_4, N_2, and H_2S impurities. *J. Chem. Thermodyn.* **2012**, *44*, 5−12.
(22) Steinbrecher, T.; Mobley, D. L.; Case, D. A. Nonlinear scaling schemes for Lennard-Jones interactions in free energy calculations. *J. Chem. Phys.* **2007**, *127*, 214108.
(23) Conde, M. M.; Vega, C. Determining the three-phase coexistence line in methane hydrates using computer simulations. *J. Chem. Phys.* **2010**, *133*, 064507.
(24) Vatamanu, J.; Kusalik, P. G. Molecular insights into the heterogeneous crystal growth of sI methane hydrate. *J. Phys. Chem. B* **2006**, *110*, 15896−15904.
(25) Vatamanu, J.; Kusalik, P. G. Heterogeneous crystal growth of methane hydrate on its sII [001] crystallographic face. *J. Phys. Chem. B* **2008**, *112*, 2399−2404.
(26) Liang, S.; Kusalik, P. G. The mobility of water molecules through gas hydrates. *J. Am. Chem. Soc.* **2011**, *133*, 1870−1876.
(27) McLaurin, G.; Shin, K.; Alavi, S.; Ripmeester, J. A. Antifreezes as catalysts of hydrate formation from ice. *Angew. Chem., Int. Ed.* **2014**, DOI: 10.1002/anie.201403638.
(28) Vu, T. H.; Gloesener, E.; Choukroun, M.; Ibourichene, A.; Hodyss R. Experimental study on the effect of ammonia on the phase behavior of tetrahydrofuran clathrates. *J. Phys. Chem. B* **2014**, 10.1021/jp5042487.